Supporting Information for:

Enhanced Photoelectrochemical Nitrogen Reduction to Ammonia by a Plasmon-Active Au Grating Decorated with gC_3N_4@MoS_2 Heterosystem and Plasmon-Active Nanoparticles

D. Zabelin[*, a], A. Tulupova[a], A. Zabelina[a], A. Tosovska[a], R. Valiev[b], R. Ramazanov[b], D. Mares[c], V. Jerabek[c], V. Burtsev[a], M. Erzina[a], A. Michalcová[d], A. Skvortsova[a], V. Svorcik[a], O. Lyutakov[a]

[a] *Department of Solid State Engineering, University of Chemistry and Technology, 16628 Prague, Czech Republic*
[b] *Department of Chemistry, University of Helsinki, FI-00014 Helsinki, Finland*
[c] *Department of Microelectronics, Czech Technical University, Prague, 16600 Czech Republic*
[d] *Department of Metals and Corrosion Engineering, University of Chemistry and Technology, 16628 Prague, Czech Republic*

* *Corresponding author: denis.zabelin@vscht.cz*

Experimental Section

Materials

Sodium molybdate dihydrate (≥ 98.0 %), thioacetamide (ACS reagent, ≥ 99.0 %), thiourea (ACS reagent, ≥ 99.0%), urea (ACS reagent, 99.0-100.5 %), hydrazine hydrate (N_2H_4, 50-60 %), $^{14}N_2$ gas (99.999 %), Ar gas (99.999 %), air (99.999 %), $^{15}N_2$ (98 at. % of ^{15}N), ammonium photometric kit test (0.010-3.00 $mg.L^{-1}$ (NH_4^+)), Spectroquant, Supelco, Merck Supelco), deionized water, ethanol (absolute), silver nitrate ($AgNO_3$, ACS reagent, ≥ 99.0 %), sodium citrate dihydrate (FG, ≥ 99.0 %), sodium borohydride ($NaBH_4$, powder, ≥ 98.0 %), bis(p-sulfonatophenyl)phenylphosphine dihydrate dipotassium salt (97.0 %), L-Cysteine (97.0 %), gold(III) chloride trihydrate (≥ 99.9 % trace metals basis), Sodium citrate tribasic dihydrate (Na_3CA, ACS reagent, ≥ 99.0 %), L-ascorbic acid (≥ 99.0 %), silver nitrate ($AgNO_3$, 99.0 %) and hexadecyltrimethylammonium bromide (CTAB, ≥ 98.0 %) were purchased from Sigma-Aldrich. DVD-R disks as periodic substrates were purchased from Verbatim (USA). Au target for magnetron sputtering was purchased from Safina (purity of 99.99 %, Czech Republic).

Sample preparation

Preparation of gC_3N_4 nanosheets. The gC_3N_4 nanoflakes were synthesized by annealing 10 g of urea at 550 °C for 4 hours (heating rate of 5 °C min^{-1}) in an air atmosphere. The resulting gC_3N_4 powder was subjected to delamination in an ice-cold ultrasonic bath in isopropanol medium for 6 hours, after which the suspension was allowed to sediment for one hour. The supernatant was then

carefully collected and the powder was separated from the suspension by centrifugation. The resulting powder was dried at 60 ℃ under ambient conditions.

Preparation of gC_3N_4@MoS_2 nanosheets. 90 mg of gC_3N_4 nanoflakes were added to 25 mL of an aqueous solution containing 0.12 g sodium molybdate dihydrate and 0.075 g thiourea. The resulting suspension was subjected to ultrasonic treatment for 30 min under nitrogen gas purging. Further suspension was placed in a Teflon-lined autoclave with subsequent heating under 200 ℃ for 18 hours. The resulting gC_3N_4@MoS_2 was washed with DI water and absolute ethanol several times and finally dried under 60 ℃ in vacuum. To obtain 2D nanosheets of gC_3N_4@MoS_2, resulting powder was immersed in liquid nitrogen for 20 min and then immediately subjected to ultrasonic treatment in ethanol medium for 1 hour. The resulting supernatant was gently collected and dried under vacuum for further use. For comparison analyses, MoS_2 nanoflakes were also prepared by the same procedure but without the addition of gC_3N_4 powder.

Preparation of periodic gold grating. The periodic gold grating was prepared using the same technique as in our previously published work [S1, S2]. Briefly, DVD-R disks were separated and washed using methanol, then a gold layer with previously selected optimal parameters (40 mA, 300 s) was deposited on their surface by magnetron sputtering.

Deposition of gC_3N_4@MoS_2 on Au grating surface. The deposition of the 2D/2D gC_3N_4@MoS_2 heterostructure onto plasmon-active periodic structure surface was carried out by electrophoresis. Since gC_3N_4@MoS_2 system has a negative charge on the surface in ethanol, a two-electrode electrochemical cell was assembled, where Pt was used as the anode and previously prepared Au grating was used as the anode. Materials deposition was carried out by applying a potential of 60 V using a suspension with ethanol for 60 minutes. The resulting sample was then carefully removed from the electrochemical cell and dried under vacuum.

Nanoparticles preparation.

Preparation of spherical Au nanoparticles

Gold nanoparticles were synthesized by a Turkevich method. 100 mL of boiling water was added to a 250 mL round bottomed flask that contained 1 mL of $HAuCl_4$ (100 mg in 10 mL) and 2.5 mL of Na_3CA (284.9 mg in 25 mL). The solution turned red after 10 min of steady heating. After, AuNPs were separated by centrifugation (7800 rpm, 20 min each cycle) and washed with water.

Preparation of cubic Au nanoparticles

Firstly, for the synthesis of spherical Au nuclei, 0.25 mL of 0.01 M gold(III) chloride solution, 7.5 mL of 0.1 M CTAB solution and 0.8 mL of 0.01 M $NaBH_4$ solution were prepared using automatic pipettes in a round bottom flask. The mixed solution was reacted for 3 hours at 30 °C. After 3 hours,

the solution was diluted 1:9 and used for further synthesis. The suspension was light brown in color. Then, the mixed solution for the cubic nanoparticles preparation consists of 8 mL of DI water, 1.6 mL of 0.1M CTAB solution, 0.2 mL of 0.01 M gold(III) chloride solution, 0.95 mL of 0.1M ascorbic acid solution, and 5 mL of the spherical gold nanoparticles suspension prepared from the previous step. This solution was reacted for 20 minutes in the dark. After 20 min, the solution was centrifuged (4000 rpm, 10 min) and washed with water for chromatography several times and used for further investigations (pink color) [S3].

Preparation of spherical Ag nanoparticles

10 mL of 0.005 M $AgNO_3$, 0.02 M sodium citrate, 0.02 M $NaBH_4$ and 0.005 M BSPP (bis(p-sulfonatophenyl)phenylphosphine dihydrate dipotassium salt) solutions were prepared first. The $NaBH_4$ solution was cooled before the synthesis. The synthesis of spherical Ag nanoparticles was carried out in a 100 mL Erlenmaier flask by adding 96 mL of DI water and 1 mL of previously prepared $AgNO_3$ solution under constant stirring. Then 1 mL of sodium citrate, $NaBH_4$ and BSPP solutions were added under vigorous stirring. The flask was covered by non-transparent material and left stirring for 30 min. After 30 min of stirring in the dark, the solution became light yellow in color.

Preparation of triangle Ag nanoparticles

The synthesis of triangle Ag nanoparticles was carried out by the same methodology as in synthesis of spherical Ag NPs but under LED lamp irradiation (595 nm, 800 mW) for 2 hours [S4].

Preparation of urchin-like Au nanoparticles

Urchin-like gold nanoparticles (AuNUs) were synthesized by seed growth method with some modifications [S5, S6]. Briefly, seed solution was prepared by mixing boiling $HAuCl_4 \cdot 4H_2O$ solution (1 mM, 100 mL) with 1 % citrate solution (15 mL) under vigorous stirring. The solution was boiled 15 min, cooled, filtered by a 0.22 μm nitrocellulose membrane and kept in a dark, cold place. AuNUs were prepared by adding the seed solution (100 μL) to $HAuCl_4$ solution (0.25 mM, 10 mL) with HCl (1 M, 10 μL). After that $AgNO_3$ (20 mM, 100 μL) and L-ascorbic acid (100 mM, 50 μL) were added simultaneously. After colour change AuNUs were immediately centrifugal washed.

Plasmon coupled system preparation

To prepare the Au/gC_3N_4@MoS_2/MeNPs system, the previously obtained Au grating/gC_3N_4@MoS_2 sample was used as a substrate for nanoparticles deposition using drop deposition methods (metal particles were previously re-dispersed in methanol).

Finite-difference time-domain calculations of E-field spatial intensity distribution

Full numerical simulations using the Finite-difference time-domain (FDTD) method were employed to investigate the local plasmon-related E-field spatial intensity distribution and plasmon strength quantified by power flow through the simulation domain of the prepared structure. The process is based on the direct solution of Maxwell's curl equations. The power flow through the simulation domain is defined as

$$S(t) = \frac{1}{S_0} Re\left[\int_A \left[E(t) \times H^*(t)\right] \cdot dA\right]$$

where E and H are the electric and magnetic fields and S_0 is the launch power. The integral is evaluated over an area A.

The basic simulated structure consisted of a bottom polymer grating template with a grating and a middle 25 nm thick Au layer covered with a thin semiconductor layer on which various NPs are deposited in water solution, forming a top layer of the simulation domain. The size of the NPs has been set to the values of the statistical distribution given by the experiment. The simulation domain always encompassed one full period of the grating with deposited NPs. The periodic boundary condition (PBC) was chosen such that the simulation is equivalent to an infinite structure composed of the basic computational domain repeated endlessly in dimension along grating vector K. At the other interfaces the perfectly matched layer (PML) was used to absorb the energy without inducing reflections.

Due to the NPs size and even smaller inter-particle distances given by the optimal coverage ratio, the very simulation fine uniform spatial grid of 0.02 nm was used. The broadband spectral absorption for all structures was simulated. The local value of coupled plasmon strength and plasmon-related electric field was then probed at the excitation wavelength of 600 nm by TM polarized light. The optical constants applicable for the VIS light region: refractive index and extinction coefficient of polycarbonate template, MoS_2 layer, and Au, Ag NPs used in the model were taken from references [S7-S9] respectively. To obtain a stable simulation, the time step was chosen to adhere to the Courant condition which relates the spatial and temporal step.

$$c\Delta t < \frac{1}{\sqrt{\left(\frac{1}{\Delta x^2} + \frac{1}{\Delta y^2} + \frac{1}{\Delta z^2}\right)}}$$

where c is the velocity of light and, for the case of a non-uniform grid, the grid sizes represent the smallest grid size in the simulation.

Density functional calculation of plasmon-assisted NRR.

DFT analysis was used to obtain insights into the NRR activity of gC_3N_4@MoS_2 heterostructure under different external e-fields. For the MoS_2 flake description, we used a bulk structure placed in 35×35×15 $Å^3$ size box with periodic boundary conditions in the XY plane. The structure of gC_3N_4 was placed under the relaxed MoS_2 structure and carried out the optimization without any constraints. Next, for calculating the free energy profile of the reduction of the N_2 molecule we used a uniform e-field near the reaction site ranging from 0 to 75 kV/m corresponding to the various types of considered nanoparticles.

The DFT calculations were carried out with the CP2K package [S10]. The DFT calculations used the combination of the Gaussian and plane-wave (GPW) [S11] scheme for electronic density representation, double-ζ valence plus polarization (DZVP) basis sets of the MOLOPT [S12] type to describe the valence electrons and norm-conserving Goedecker-Teter-Hutter (GTH) [S13] pseudopotentials to approximate the core electrons. The generalized gradient approximation (GGA) of the Perdew−Burke−Ernzerhof (PBE) [S14] functional was used to describe the exchange-correlation interactions. DFT-D3 method [S15] was adopted to consider the van der Waals (vdW) interaction. For the MoS_2 flake description, we used bulk structure placed in 35×35×15 $Å^3$ size box with periodic boundary conditions in the XY plane. The structure of gC_3N_4 was placed under the relaxed MoS_2 structure and carried out the optimization without any constrains.

To calculate the free energy profile of the reduction of the N_2 molecule, we used:

$$\Delta G = \Delta E + \Delta E(ZPE) - T\Delta S,$$

where ΔE is the absorption energy, $\Delta E(ZPE)$ is the zero-point energy difference, and $T\Delta S$ is the entropy difference between the hydrogenation steps. For adsorbates, ZPE and S are determined by vibrational frequencies calculations. For molecules, those are taken from the NIST database [S16].

Measurement techniques

Materials characterization

Fourier transform infrared (FTIR)–attenuated total reflection (ATR) spectra were recorded using a Nicolet 6700 spectrometer (Thermo Scientific, France) with a Smart ATR accessory device (1500 scans and 4 cm^{-1} resolution). Raman spectra were measured with a Thermo Scientific Raman dispersion spectrometer - model DXR Microscope, equipped with an Olympus confocal microscope. An 532 nm excitation wavelength and an input power of 10 mW were used. X-ray photoelectron spectroscopy (XPS) was performed using an Omicron Nanotechnology ESCAProbeP spectrometer with a monochromated Al K Alpha X-ray source operating at 1486.6 eV. The energy resolution was 0.4 eV for the survey study and 0.1 eV for the high-resolution XPS spectra measurements. X-ray diffraction microscopy spectra were recorded on a microXRD D8 Discover

diffractometer for 30 min using Cu Kα radiation (1.5405 Å). SEM-EDX images (LYRA3 GMU, Tescan, CR) were obtained at 30 mA and 40 kV accelwerating voltage, energy dispersive spectroscopy was performed with utilization X-MaxN, 20 mm^2 SDD detector, Oxford instruments. The atomic force microscopy (AFM) surface topographies were measured using the Icon system (Bruker) in Peakforce mode. UV-Vis absorption spectra were obtained on a Lambda 25 UV/Vis/NIR Spectrometer (PerkinElmer, USA). HRTEM measurements were performed using an EFTEM Jeol 2200 FS microscope (Jeol, Japan). The determination of NMR-based ammonia was provided by using a Bruker 600 AvanceIII (pulse sequence zgpr; 512 scans). Typically, 125 μL of the standard solution was mixed with 50 μL of 4 M H_2SO_4 in DMSO-d_6 and 750 μL of DMSO-d_6 before doing an instantaneous analysis. The rate of H_2 evolution was measured by GC-7920 (Agilent) gas chromatography system.

Electrochemical measurements

In photo-electrochemical experiments samples catalytic activities toward NRR were studied by linear sweep voltammetry, impedance spectroscopy and chronoamperometry. All electrochemical measurements were performed in H-type cell at room temperature under illumination with LED (595 nm wavelength) or in dark, both with portable potentiostat PalmSens 4 (Palm Instruments, Netherlands) in a three-electrode cell. The sample was used as the working electrode, Pt as the counter electrode and Ag/AgCl as the reference electrode. Before the test, the Nafion 211 membrane, used as a separator in H-cell, was pretreated with 3.0 % H_2O_2 and dilute 0,5 M H_2SO_4 under 80 °C for 1 h, followed by rinsing with DI water for several times. Highly pure nitrogen (N_2) gas was pumped into the electrolyte for 30 min before testing to remove the dissolved oxygen. N_2 gas was continuously flowed in the electrolyte during the data collecting process. Electrochemical impedance spectroscopy (EIS) was performed in 1 M KOH solution with the frequency range of 1–100 000 Hz (applied potential was 1.0 V vs. Ag/AgCl). In impedance measurements an equivalent electrical circuit, comprising solution resistance, contact interface resistance, and constant phase element was used.

Photoelectrochemical Nitrogen Reduction Reaction

All photoelectrocatalytic N_2 reduction experiments were carried out in chronoamperometric mode in 0.1 M Na_2SO_4 mixture solution which contained 20 wt. % ([C4mpyr][eFAP]) in H-type electrochemical cell, which was purged with different gases (N_2, Ar) for 30 min before the experiment and then continuously purged with nitrogen during experiments. As a light source the Solar Simulator SciSun-300, Class AAA was used, power on sample surface was adjusted to 100 $mW.cm^{-2}$). The amount of ammonia produced was determined photometrically and calculated using a calibration

curve using the KIT test in the concentration range 0-3 mg.L^{-1} (see Fig. S20). It should be considered that NH_4^+ concentration values depend on the pH value of the solution, so all obtained values were correlated according to ammonium cations concentration in the model solutions.

Detection of N_2H_4

The determination of hydrazine N_2H_4 amount was performed by Watt and Chrisp method. The photometric solution was prepared by dissolving para-(dimethylamino)benzaldehyde (8 g) in a mixture of HCl (40 mL) and ethanol (400 mL). 5 mL of the reaction solution after the NRR process was taken from the H-type cell, added to 5 mL of the prepared photometric solution After stirring for 15 min at 25 °C, the solution was subjected to UV-Vis measurement. N_2H_4 solutions with known concentrations (in 0.1 M Na_2SO_4, containing 20 wt. % ([C4mpyr][eFAP])) were taken as calibration standards.

Stability test in NRR

Chronoamperometry (CA) was used to evaluate the stability of the sample activity. CA curves were obtained while continuously purging the reaction solution with N_2 during sunlight illumination. Seven stability cycles, each lasting 2 hours, were carried out. After each cycle, the reaction mixture was diluted and then analyzed using the photometric test. The electrochemical cell was filled with a new reaction solution, and the experiment was repeated again with the same photoelectrode. Stability tests were repeated 3 times (presented results represent averaged values of current density and ammonia produced, the standard deviation was used for error bars creation in the last case).

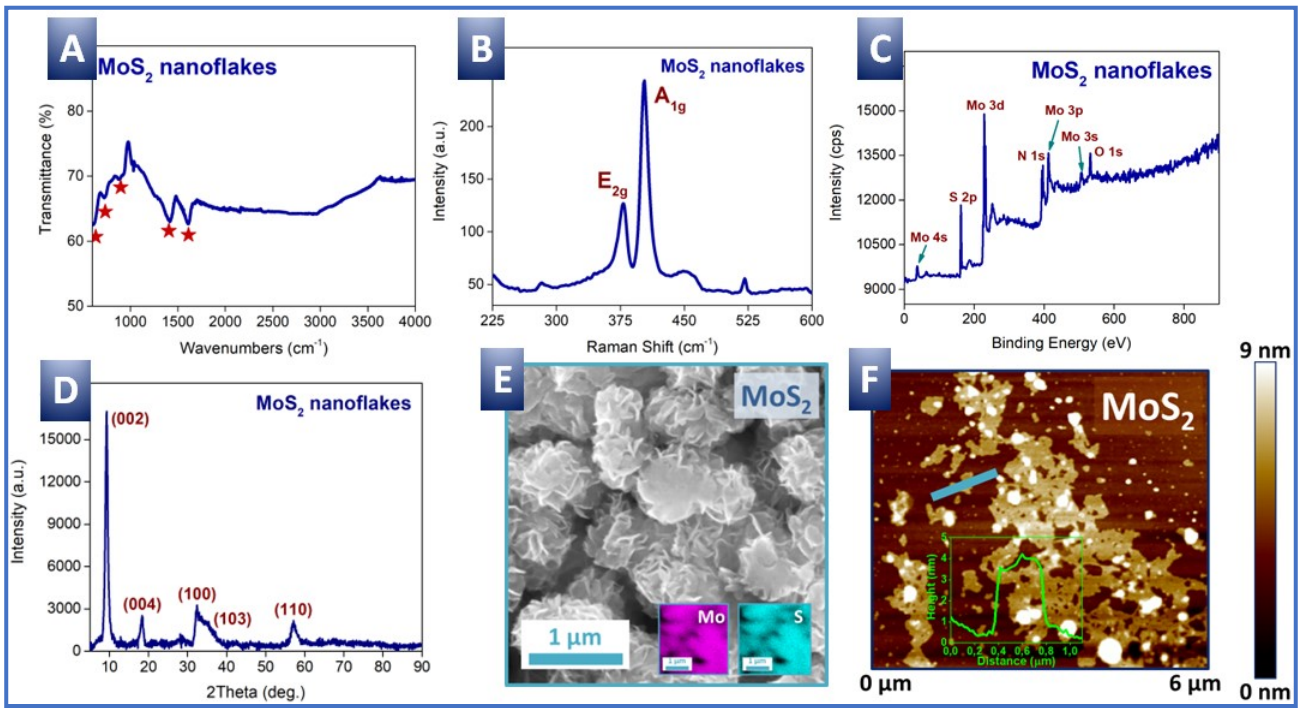

Fig. S1 Control MoS_2 characterization: (A, B, C) – FTIR, Raman, and XPS spectra; (D) – XRD pattern; (E, F) – SEM and AFM measured morphology (before and after exfoliation).

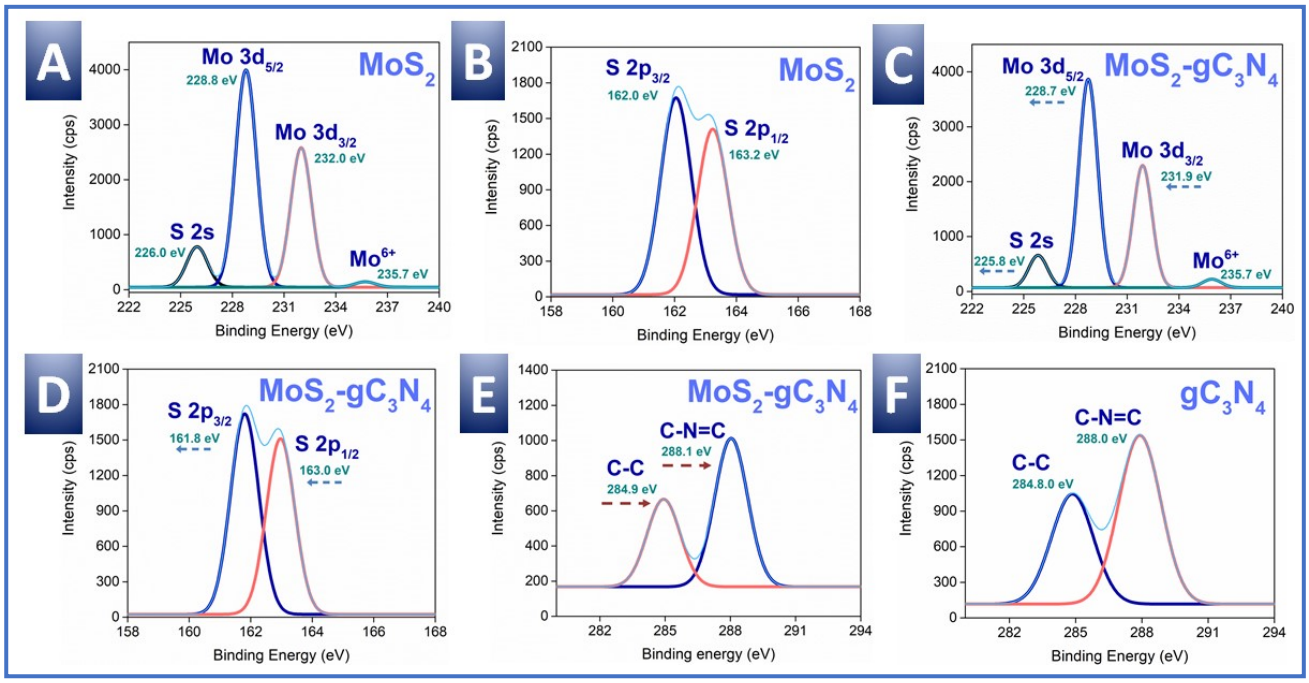

Fig. S2 High resolution XPS spectra, measured with utilization of "control" MoS_2 powder and coupled gC_3N_4@MoS_2 powder.

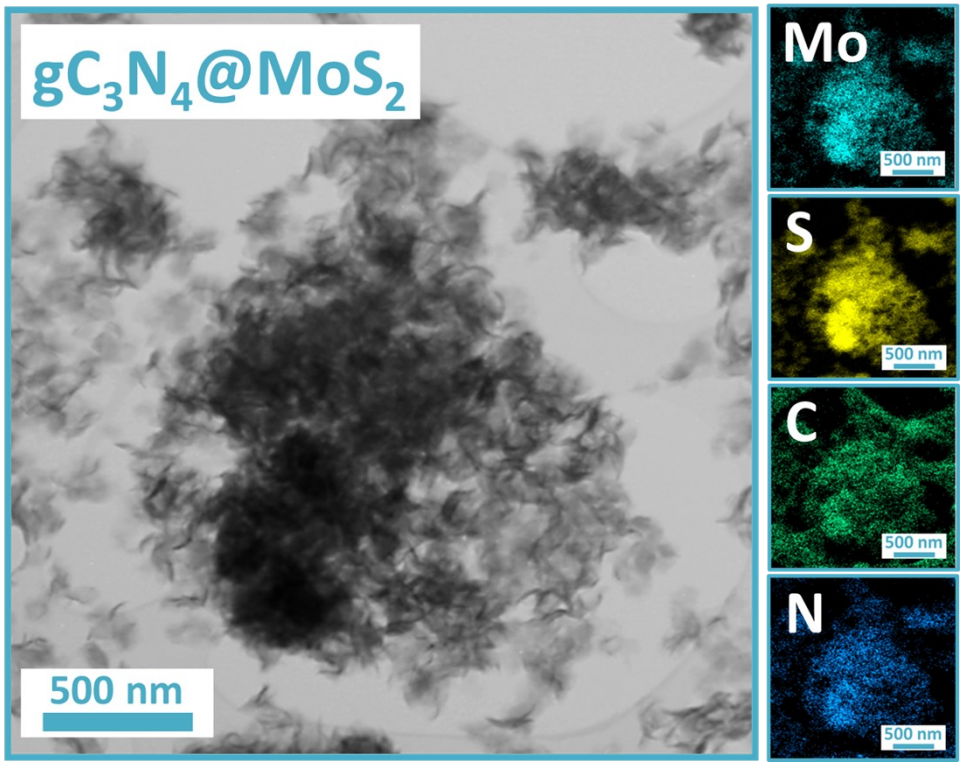

Fig. S3 HRTEM-EDX characterization of gC_3N_4@MoS_2.

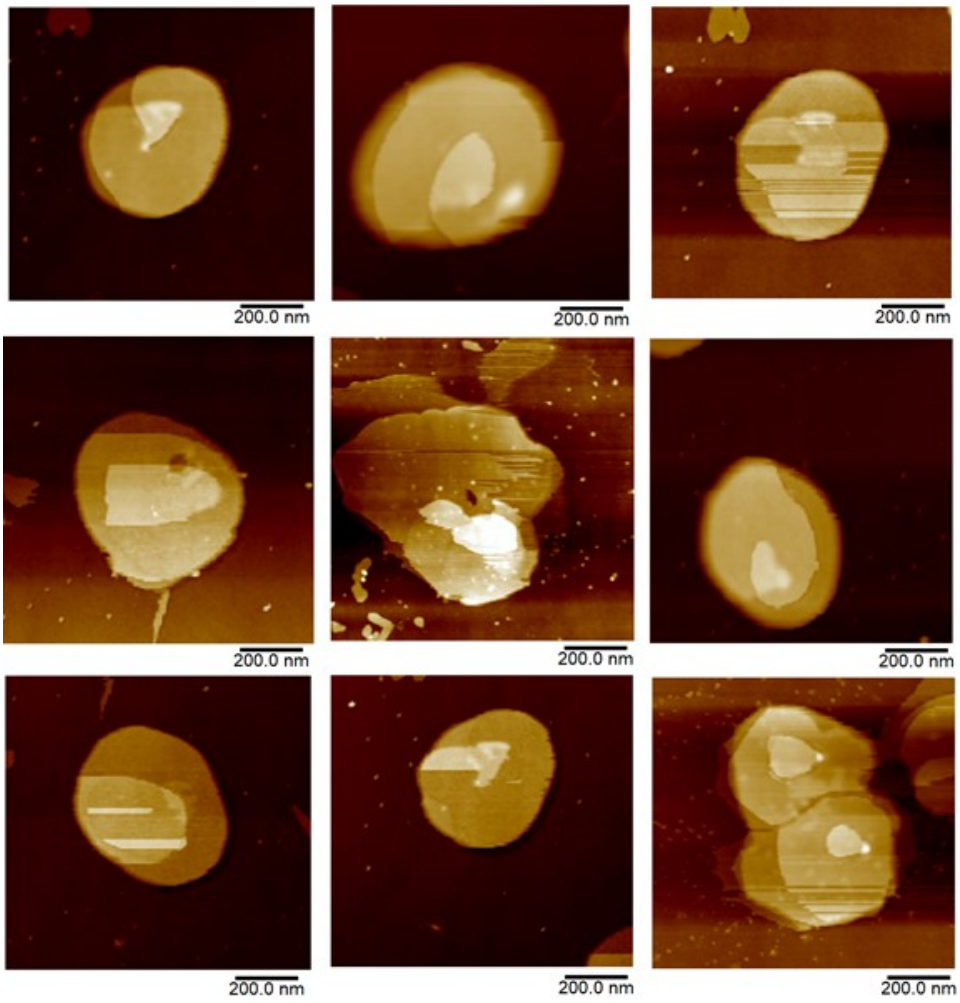

Fig. S4 AFM measured morphology of $gC_3N_4@MoS_2$ coupled structure.

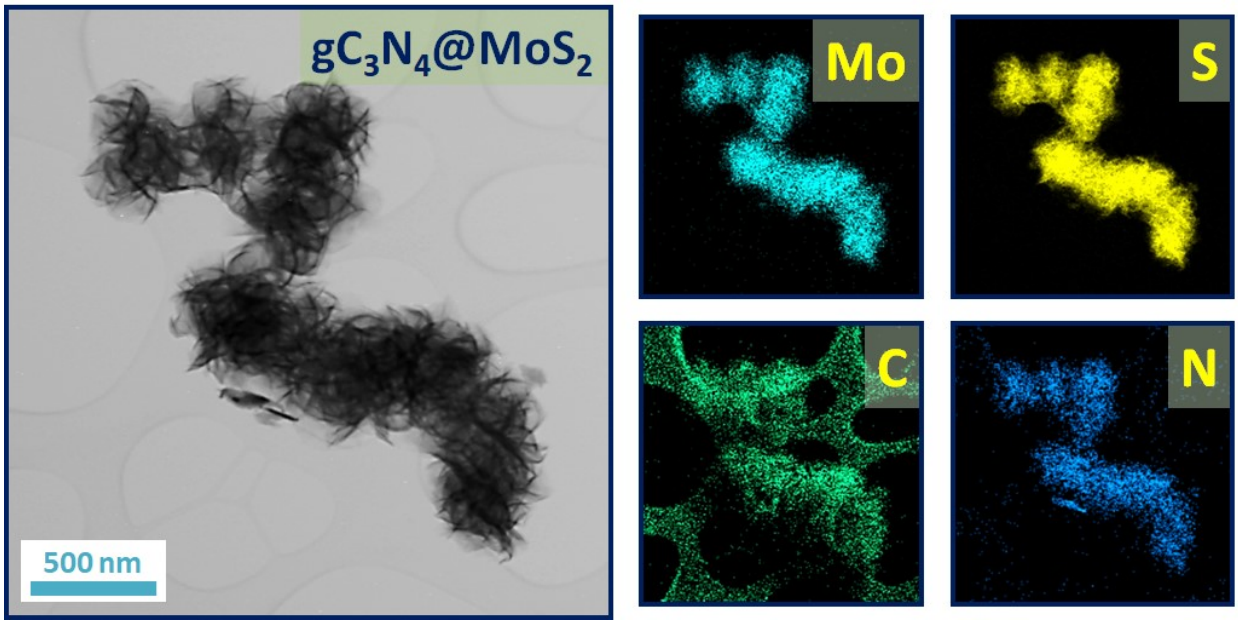

Fig. S5 HRTEM image of $gC_3N_4@MoS_2$ with HRTEM-EDX mapping of Mo, S, C and N

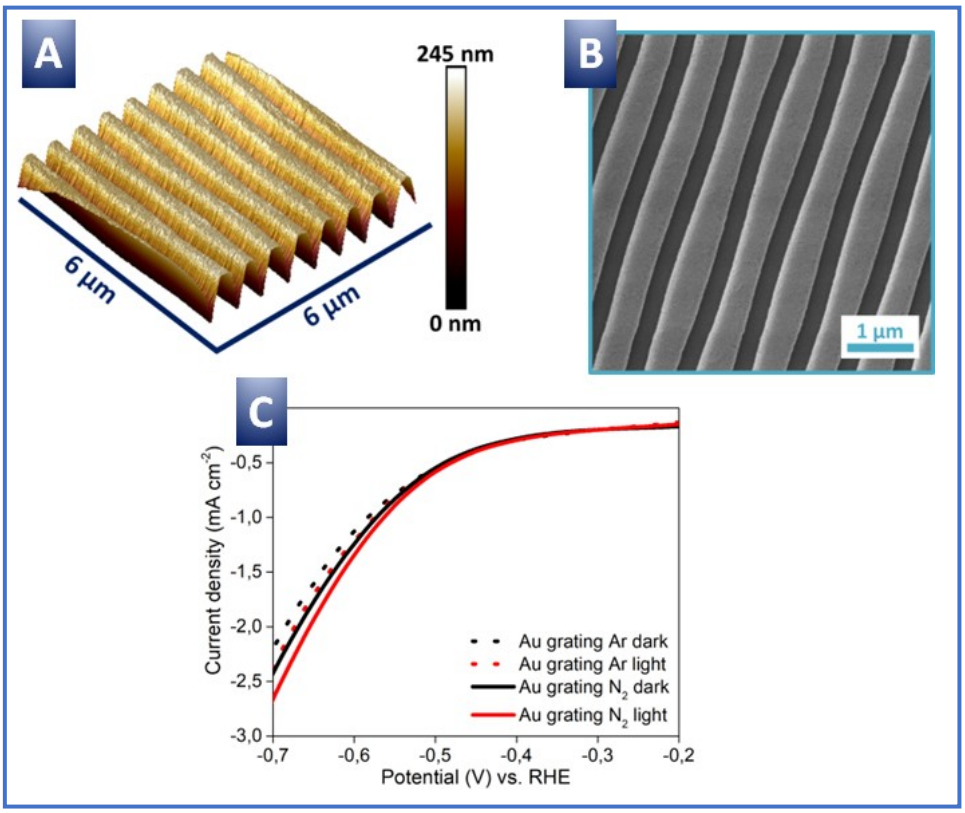

Fig. S6 Au grating morphology (AFM and SEM, top) and control LSV measurements (bottom) performed with utilization of Au grating.

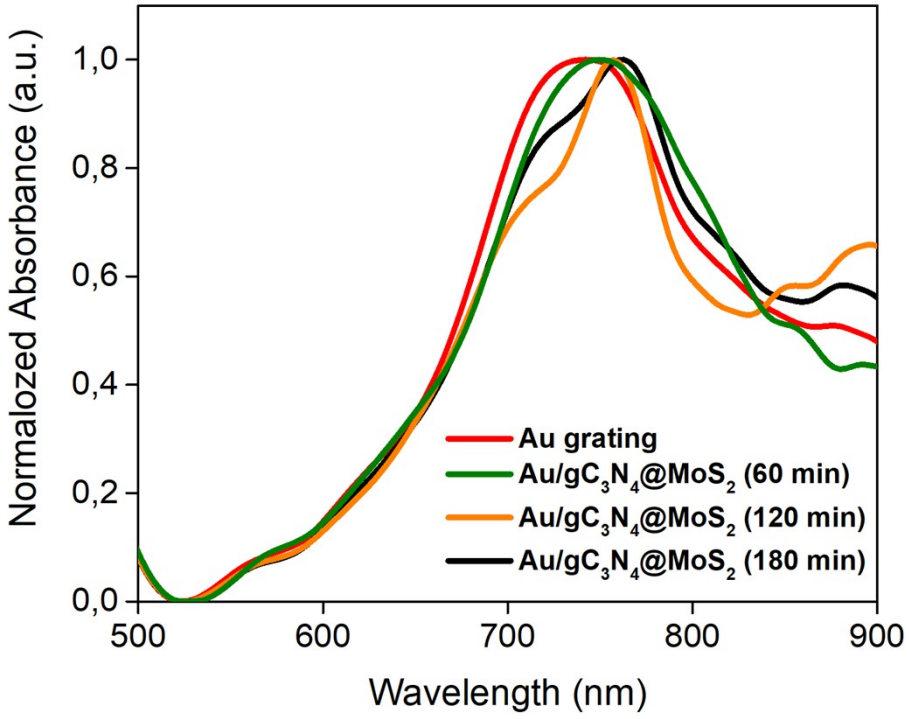

Fig. S7 Normed UV-Vis absorption spectrum of Au grating, measured at different times after the gC_3N_4@MoS_2 deposition.

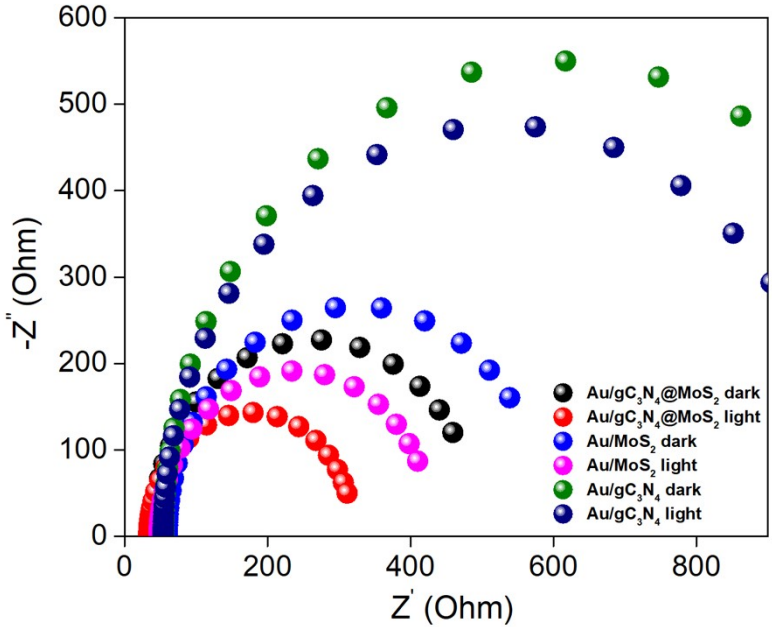

Fig. S8 EIS spectra, measured on Au/gC_3N_4, Au/MoS_2 and $Au/gC_3N_4@/MoS_2$ samples in dark or under simulated sunlight illumination.

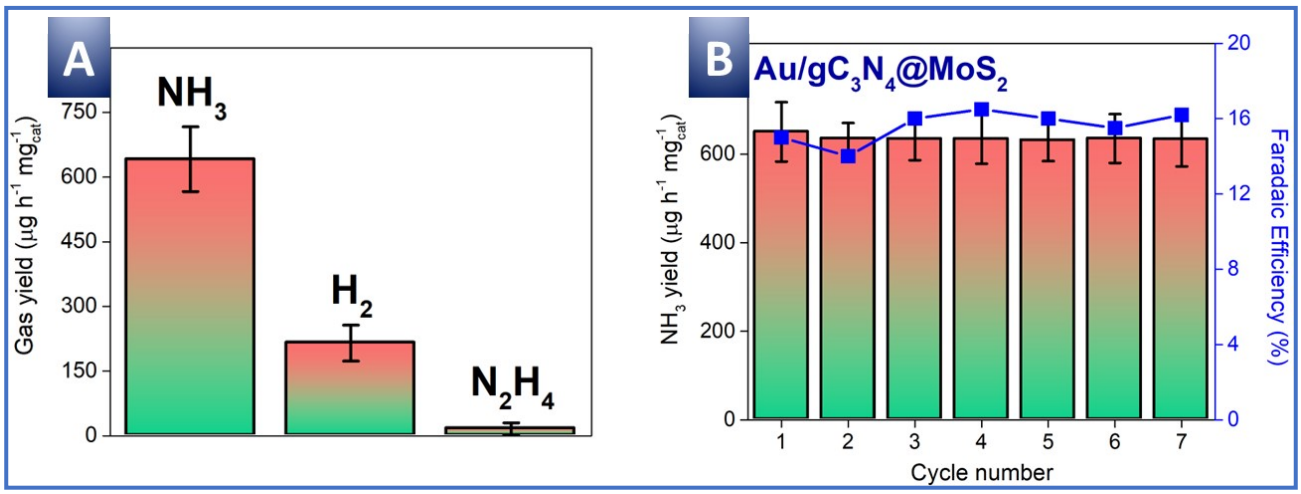

Fig. S9 (A) - NH_3, H_2, and N_2H_4 yields reached on $Au/gC_3N_4@MoS_2$ surface in photoelectrochemical mode; (B) - NH_3 yield and Faradaic efficiency obtained on $Au/gC_3N_4@MoS_2$ surface during stability tests (see Fig. 4F).

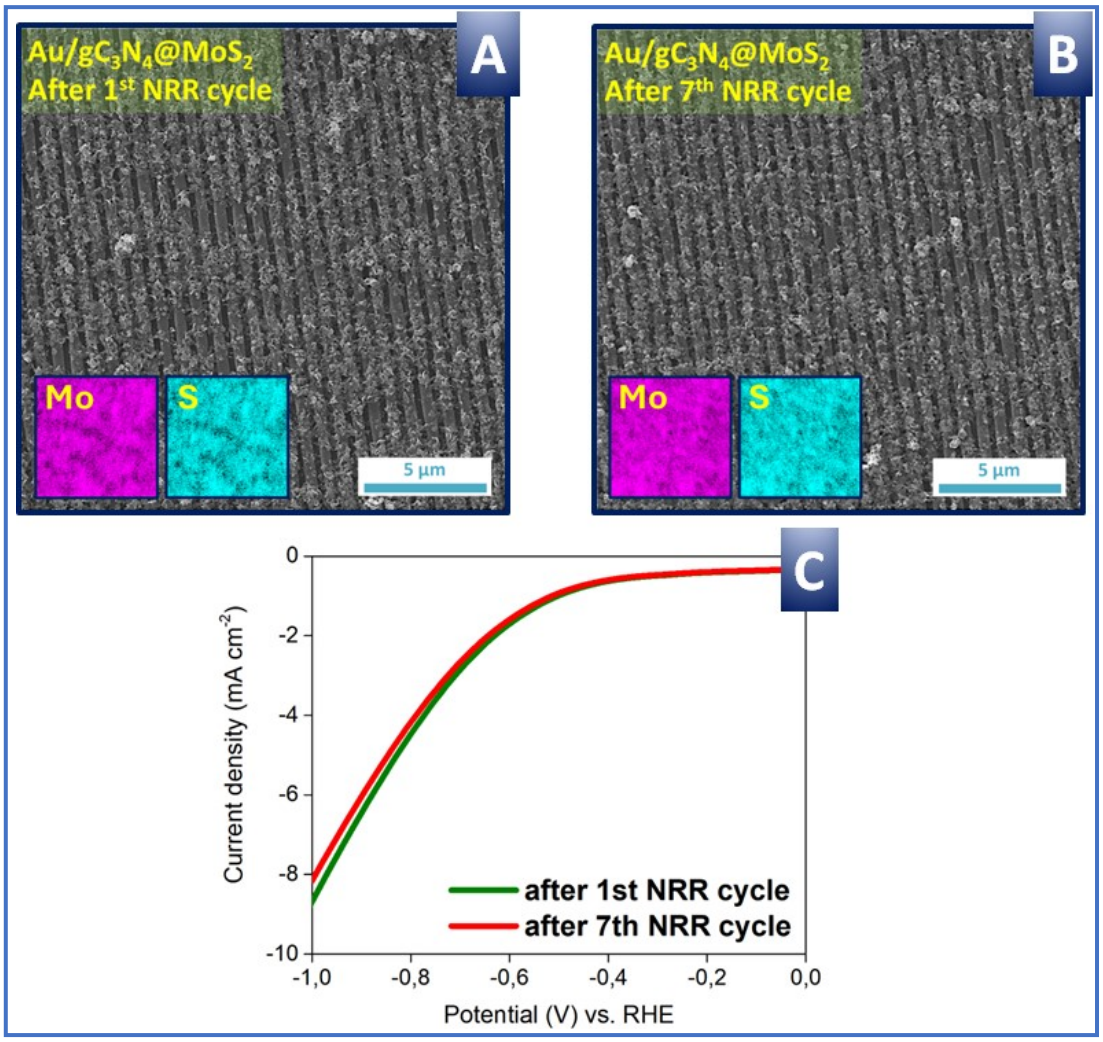

Fig. S10 Surface morphology characterization after stability test (A, B) and LSV (C) measured samples electrochemical activity.

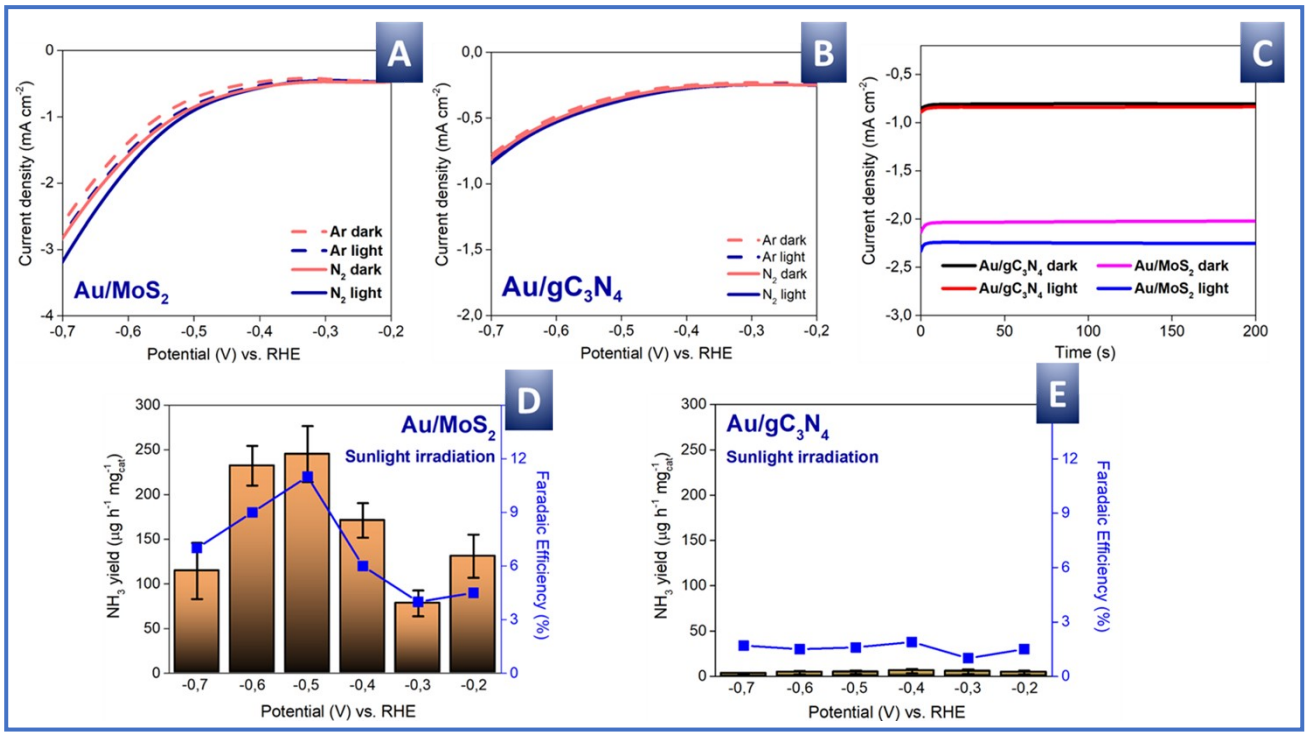

Fig. S11 Control measurements: (A, B, C) – LSV curves measured on Au/MoS_2 and Au/gC_3N_4 surface under Ar or N_2 electrolyte purging; (C) - current densities in chronoamperometry regime on Au grating/ gC_3N_4 and Au grating/MoS_2 surface (under light illumination and in the dark), NH_3 yield and faradaic efficiency obtained on Au grating/ gC_3N_4; (D) and Au grating/MoS_2 (E) surfaces.

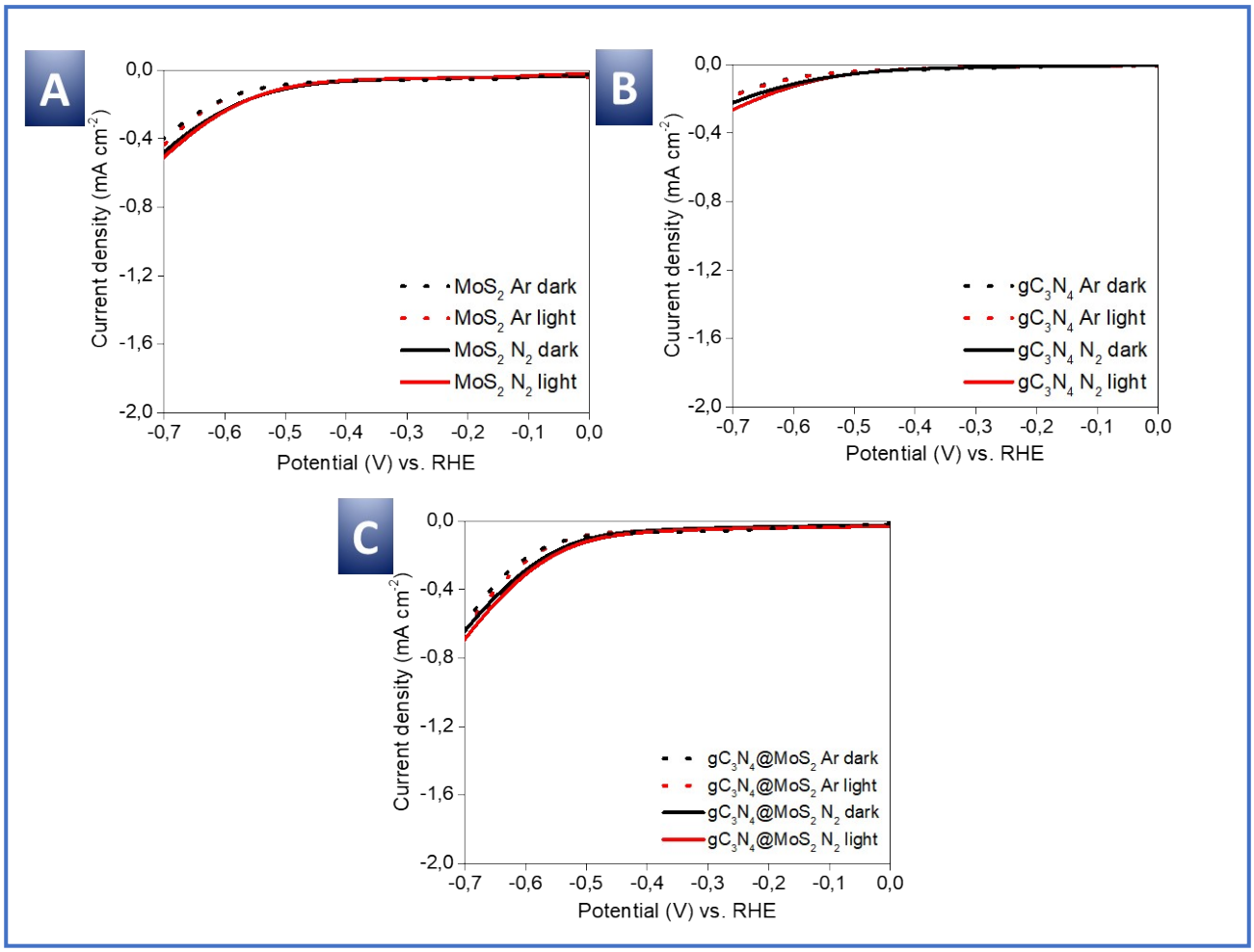

Fig. S12 Characterization of MoS_2, gC_3N_4, and gC_3N_4@MoS_2 NRR activity in LSV mode (powders were deposited on carbon electrode surface).

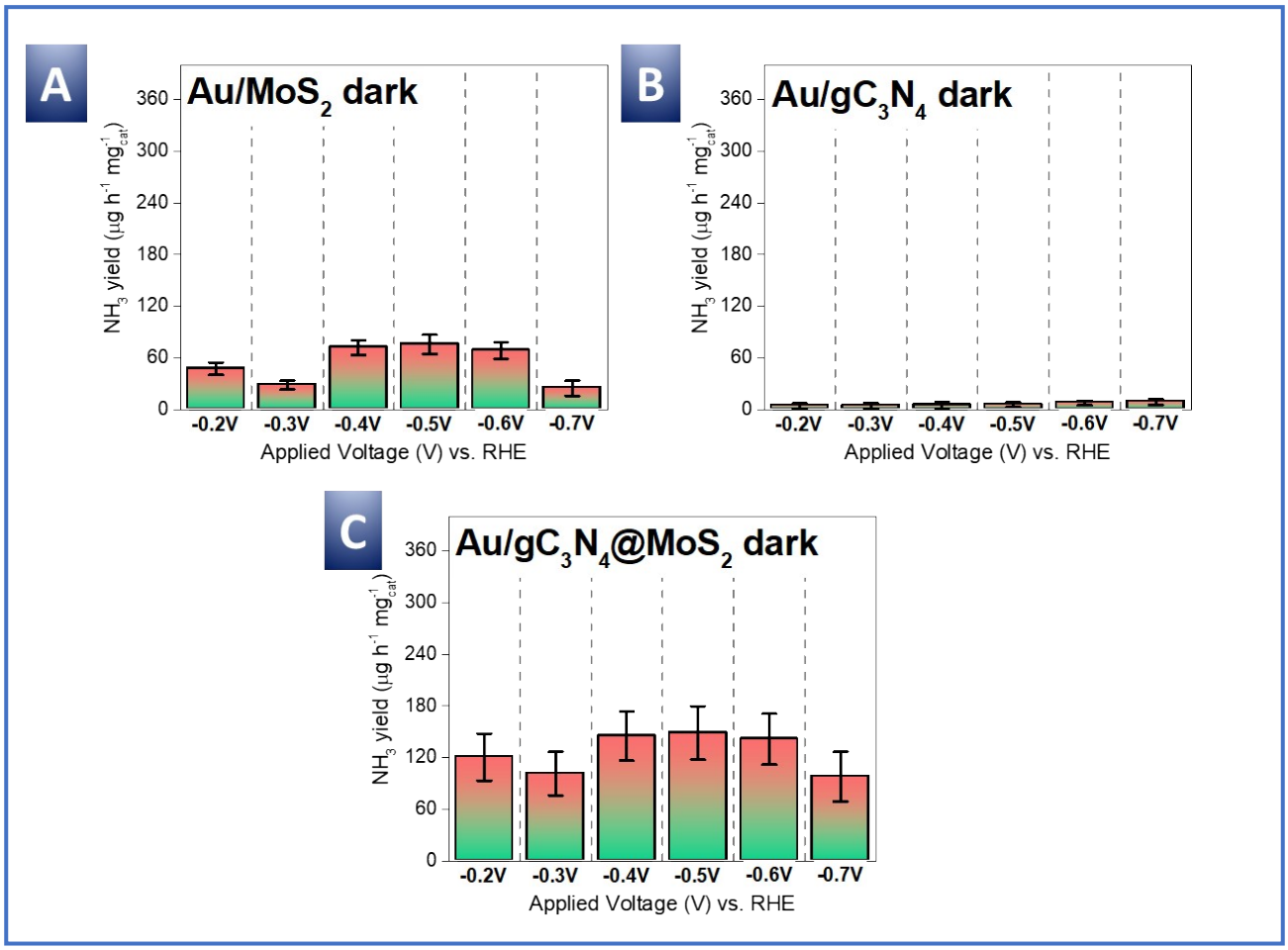

Fig. S13 NH_3 yields reached on Au/MoS_2, Au/gC_3N_4, and $Au/gC_3N_4@MoS_2$ in dark under different potentials.

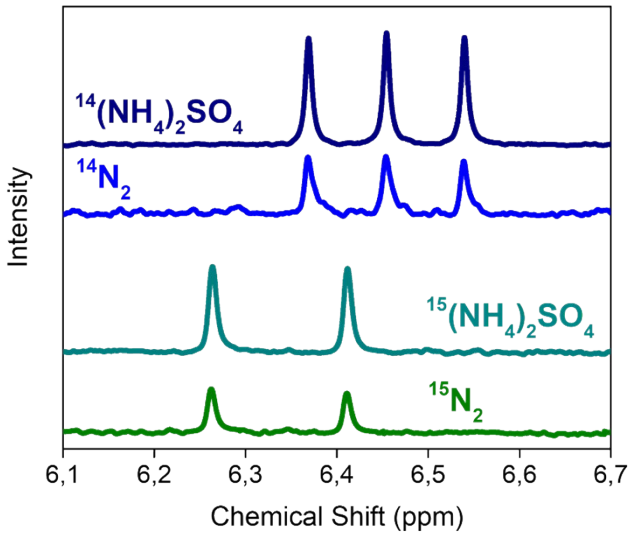

Fig. S14 Control NMR measurement of ammonia production with utilization of $^{15}N_2$ precursor and $(^{15}NH_4)_2SO_4$ salt.

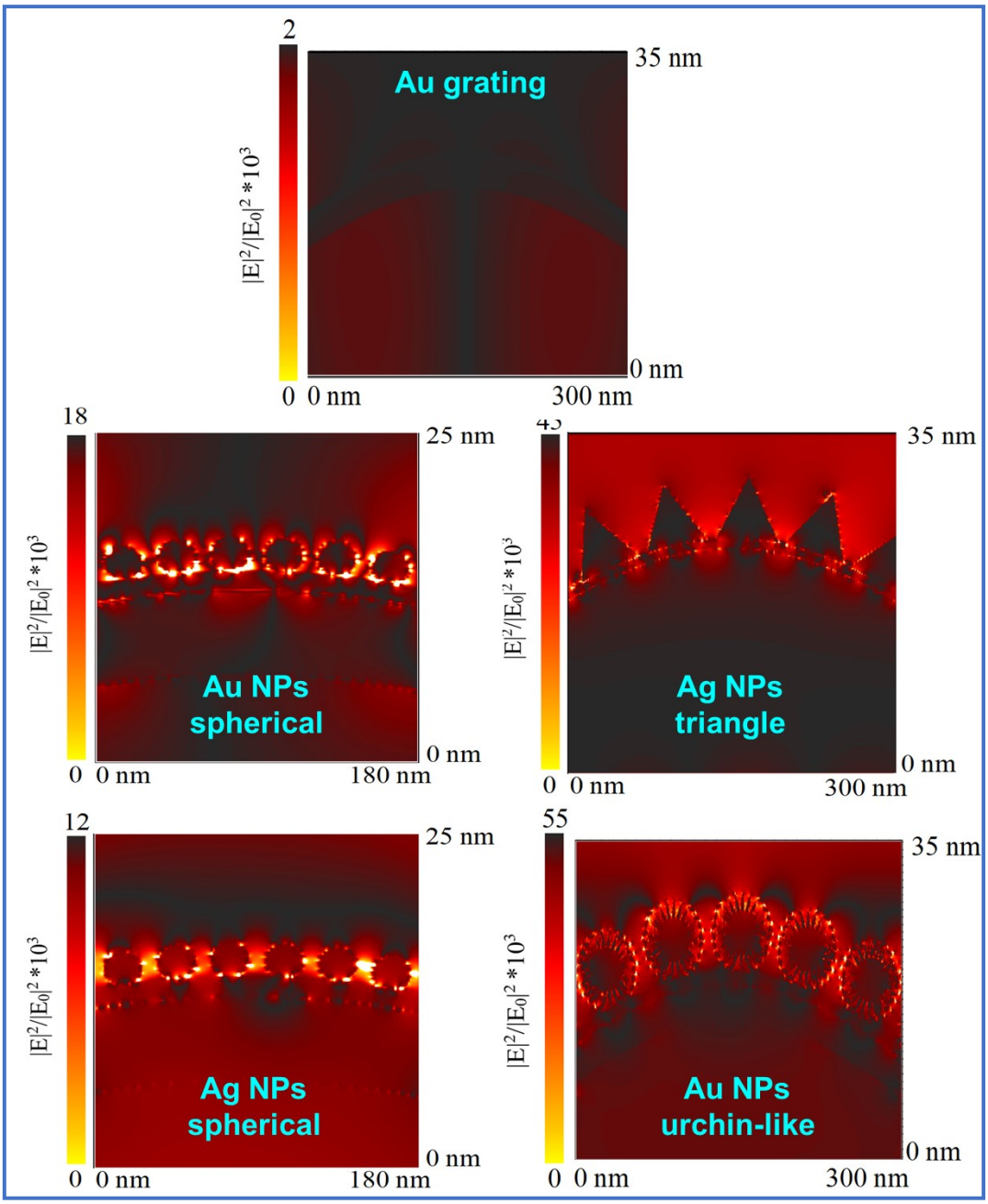

Fig. S15 Results of FDTD simulation of plasmon coupling and local values of EF between Au grating and different plasmon nanoparticles (with gC_3N_4@MoS_2 spacer).

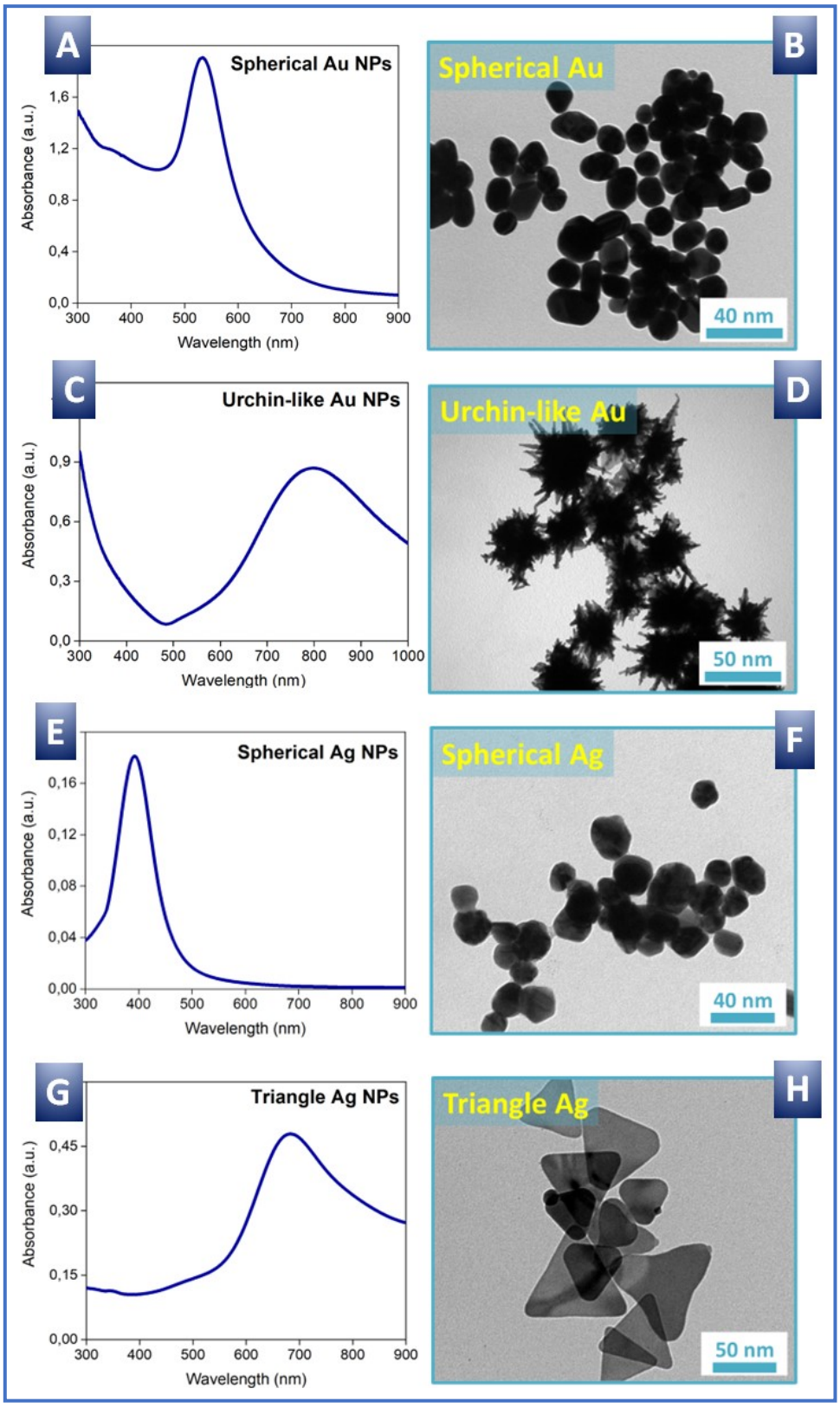

Fig. S16 UV-Vis (A, C, E, G) and TEM (B, D, F, H) of different metal nanoparticles, used for creation of coupled plasmon system.

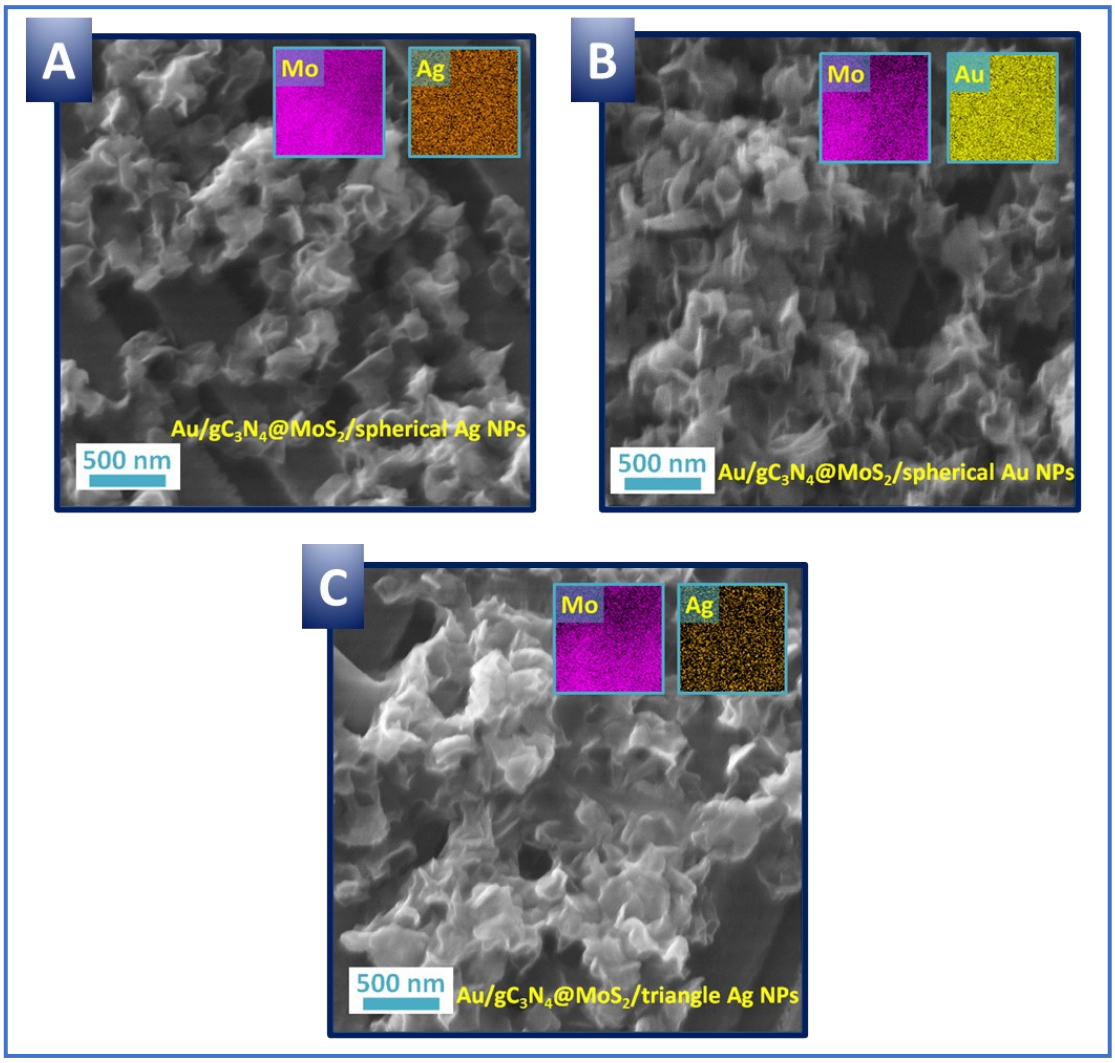

Fig. S17 SEM-EDX measurements of Au/gC_3N_4@MoS_2/MeNPs surface.

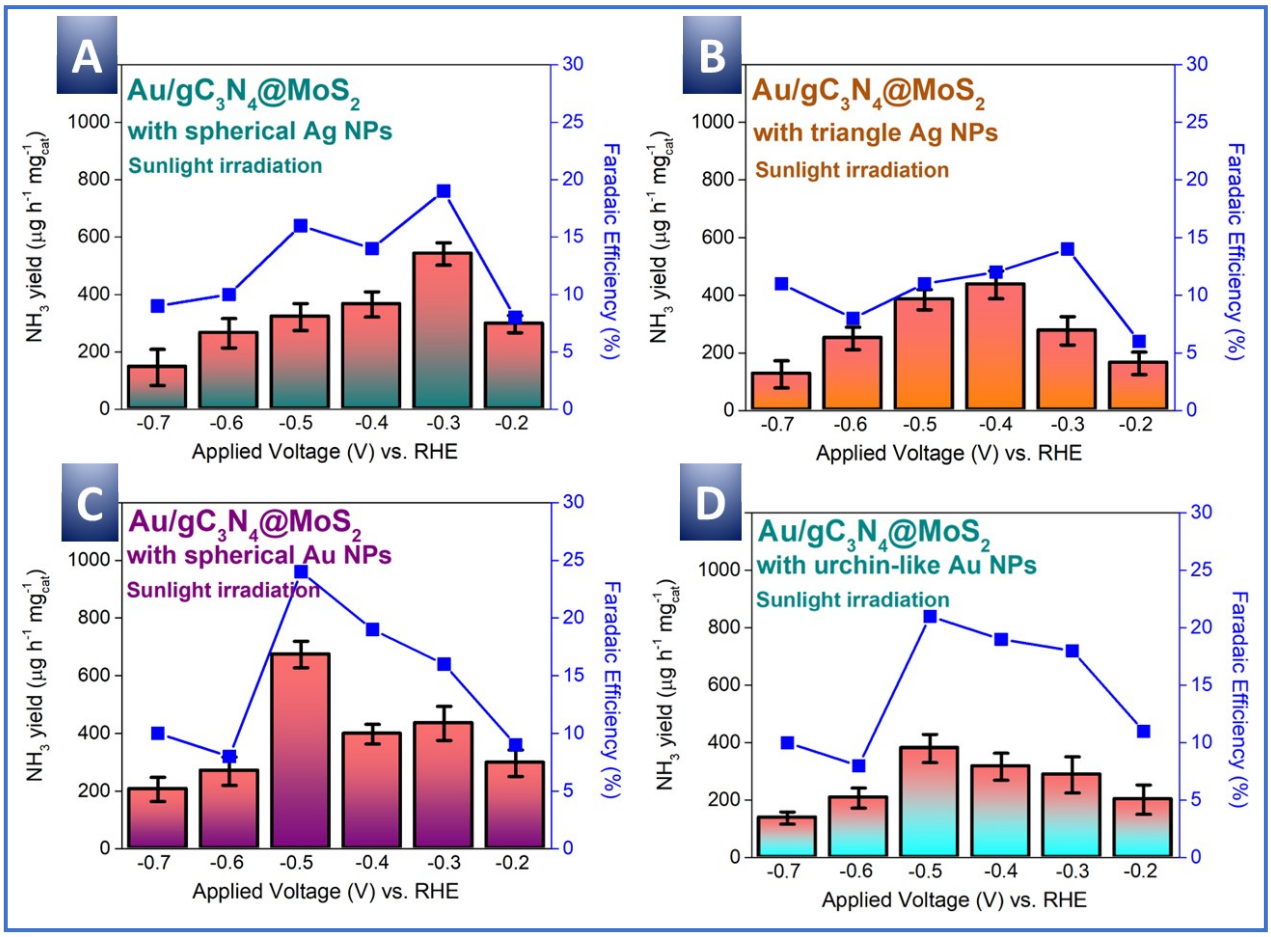

Fig. S18 NH_3 yield and faradaic efficiency reached on (A) Au grating / $gC_3N_4@MoS_2$ / spherical AgNPs, (B) Au grating / $gC_3N_4@MoS_2$ / triangle AgNPs, (C) Au grating / $gC_3N_4@MoS_2$ / spherical Au NPs, and (D) Au grating / $gC_3N_4@MoS_2$ / Au nanourchins in photoelectrochemical mode.

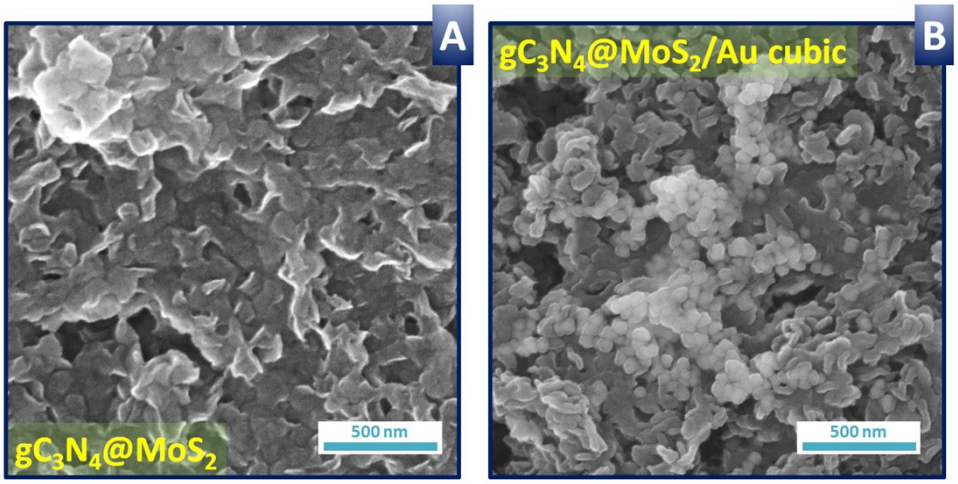

Fig. S19 Comparison of $gC_3N_4@MoS_2$ surface before (A) and after (B) deposition of Au nanocubes.

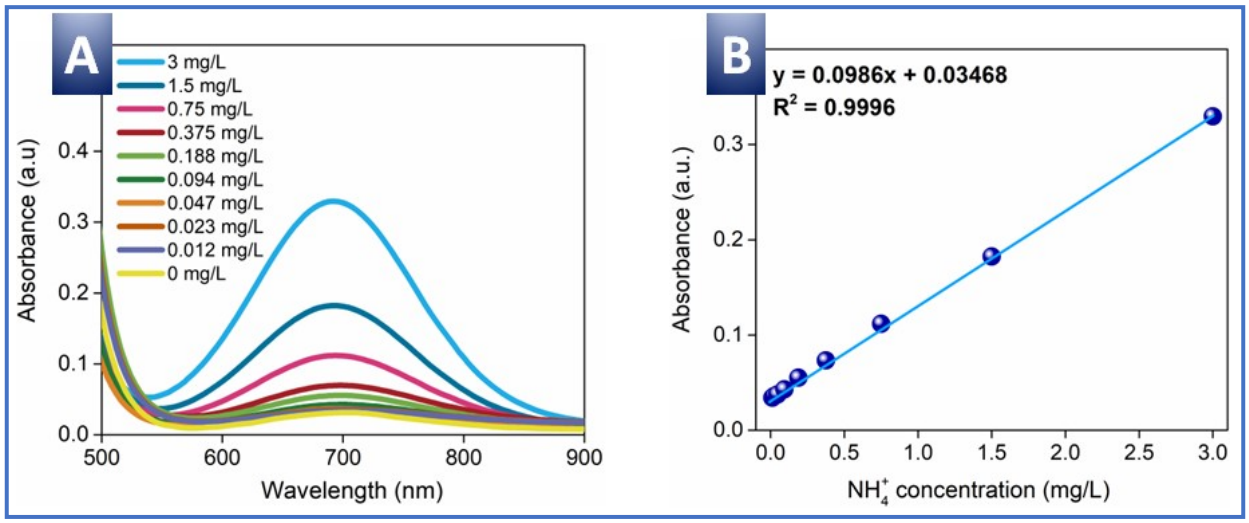

Fig. S20 UV-Vis spectra (A) and corresponded calibration curve (B) used for NRR efficiency estimation (pH correction corresponding to its value after the NRR process was achieved by adding some volume of 0.1M NaOH to the solution).

References

[S1] D. Zabelin, K. Severa, J. Kuliček, B. Rezek, A. Tulupova, R. Elashnikov, A. Zabelina, V. Burtsev, P. Sajdl, E. Miliutina, V. Svorcik and O. Lyutakov, *ACS Appl. Mater. Interfaces*, 2023, **15**, 29072–29083.

[S2] A. Zabelina, E. Miliutina, J. Dedek, A. Trelin, D. Zabelin, R. Valiev, R. Ramazanov, V. Burtsev, D. Popelkova, M. Stastny, V. Svorcik and O. Lyutakov, *ACS Catal.*, 2023, **13**, 10916–10926.

[S3] H.-E. Lee, R. M. Kim, H.-Y. Ahn, Y. Y. Lee, G. H. Byun, S. W. Im, J. Mun, J. Rho and K. T. Nam, *Nat. Commun.*, 2020, **11**, 263.

[S4] T. H. N. Nguyen, T. D. Nguyen, and M. T. Cao, *Colloid. Surfac A* 2020, **594**, 124659.

[S5] Y. Kalachyova, A. Olshtrem, O. A. Guselnikova, P. S. Postnikov, R. Elashnikov, P. Ulbrich, S. Rimpelova, V. Švorčík and O. Lyutakov, *ChemistryOpen*, 2017, **6**, 254–260.

[S6] Y. Kalachyova, D. Mares, V. Jerabek, P. Ulbrich, L. Lapcak, V. Svorcik and O. Lyutakov, *Phys. Chem. Chem. Phys.*, 2017, **19**, 14761–14769.

[S7] N. Sultanova, S. Kasarova and I. Nikolov, *Acta Physica Polonica A*, 2009, 116, 585-587

[S8] G. A. Ermolaev, Yu. V. Stebunov, A. A. Vyshnevyy, D. E. Tatarkin, D. I. Yakubovsky, S. M. Novikov, D. G. Baranov, T. Shegai, A. Y. Nikitin, A. V. Arsenin, V. S. Volkov., *NPJ 2D Mater.* Appl., 2020, 4, 21.

[S9] Aleksandar D. Rakic, Aleksandra B. Djurisic, Jovan M. Elazar, and Marian L. Majewski, *Applied Optics*, 1998, 37, 5271.

[S10] J. Hutter, M. Iannuzzi, F. Schiffmann and J. VandeVondele, *WIREs Comput. Mol. Sci.*, 2014, **4**, 15–25.

[S11] B. G. Lippert and J. H. and M. Parrinello, *Mol. Phys.*, 1997, **92**, 477–488.

[S12] J. VandeVondele and J. Hutter, *J. Chem. Phys.*, 2007, **127**, 114105.

[S13] S. Goedecker, M. Teter and J. Hutter, *Phys. Rev. B*, 1996, **54**, 1703–1710.

[S14] J. P. Perdew, K. Burke and M. Ernzerhof, *Phys. Rev. Lett.*, 1996, **77**, 3865–3868.

[S15] E. Caldeweyher, C. Bannwarth and S. Grimme, *J. Chem. Phys.*, 2017, **147**, 034112.

[S16] Johnson, R. Computational Chemistry Comparison and Benchmark Database, NIST Standard Reference Database 101, 2002.